Nickel and cobalt oxide composite as a possible electrode material for electrochemical supercapacitors

Guoping Wang [a,b,*], Lei Zhang [b,1,**], Jenny Kim [b,2], Jiujun Zhang [b,1,2]

[a] College of Chemical Engineering, University of South China, Hengyang 421001, China
[b] Institute for Fuel Cell Innovation, National Research Council of Canada, 4250 Wesbrook Mall, Vancouver, BC, Canada V6T 1W5

HIGHLIGHTS

► $Ni_{0.37}Co_{0.63}(OH)_2$ was synthesized as a possible electrode material for supercapacitors.
► A high specific capacitance of 1840 F g^{-1} was achieved in alkaline solution.
► The redox mechanism of two-electron accompanied by two OH$^-$ ion was proposed for $Ni_{0.37}Co_{0.63}(OH)_2$.

ARTICLE INFO

ABSTRACT

In this paper, a composite material, $Ni_{0.37}Co_{0.63}(OH)_2$, is synthesized using the chemical precipitation method with the purpose to develop electrode materials for supercapacitors. Physical characterization using XRD, EDX, and SEM show that $Ni_{0.37}Co_{0.63}(OH)_2$ possesses an amorphous structure, which leads to high specific capacitance of 1840 F g^{-1} in the potential window of 0–1.5 V. Cyclic voltammetry methods are employed to characterize the electrochemical properties of this electrode material in a N$_2$-saturated alkaline solution. The results demonstrate that this material could give a two-electron redox process accompanied by two OH$^-$ ions. Cyclic voltammogram curves recorded for this $Ni_{0.37}Co_{0.63}(OH)_2$ material are used to measure the specific capacitances at different potential scan rates. To validate this material for supercapacitor applications, charging/discharging tests are also conducted.

Crown Copyright © 2012 Published by Elsevier B.V. All rights reserved.

1. Introduction

The electrochemical supercapacitor (ES), as a reliable energy storage and delivery device, has drawn much attention in recent years due to its advantages such as high power density, high durability, long shelf life, flexible operating temperature, environmental friendliness, and safety [1–8]. These advantages make ES play an increasingly important role in applications such as electric vehicles, electric hybrid vehicles, digital communication devices, digital cameras, mobile phones, electric tools, pulse laser techniques, uninterruptible power supplies as well as energy storage generated by solar cells [1,9–15]. Because of this, ES has been considered as a key technology for future energy storage systems [16]. However, ES's also suffer some significant drawbacks; for instance, low energy density (commercially available ES can provide energy density of only 3–4 Wh kg^{-1}; while a battery can provide more than 50 Wh kg^{-1}) and high cost (particularly per unit of energy). Due to its low energy density, if a large energy capacity is required for an application, large ES's must be constructed, which incurs a high cost. In order to overcome this challenge, great effort has been put on developing ES electrode materials with high capacitances since high capacitance electrode materials can store more charge, leading to high energy density.

Regarding ES electrode materials, there are three major types [5,17,18]: (1) carbon materials with high specific surface areas [19,20], (2) conducting polymers [21–25], and (3) metal oxides/hydroxides such as RuO$_2$ [26,27], IrO$_2$ [28], MnO$_2$ [29,30], NiO [31,32], Co$_2$O$_3$ [33] as well as Co(OH)$_2$ [34]. These materials store energy through electric double-layer capacitances, faradaic capacitance mechanisms, or both. Unfortunately, each one of these materials may face some challenges. Carbon materials may only physically store limited charges, causing low specific capacitance (SC), conducting polymers may swell and shrink during the intercalating/deintercalating processes leading to low cycling stability,

* Corresponding author at: College of Chemical Engineering, University of South China, Hengyang 421001, China. Tel.: +86 734 8282 667; fax: +86 734 8282 375.
** Corresponding author. Tel.: +1 604 221 3087/3000x5504; fax: +1 604 221 3001.
E-mail addresses: wgpcd@yahoo.com.cn (G. Wang), lei.zhang@nrc.gc.ca (L. Zhang), jiujun.zhang@nrc.gc.ca (J. Zhang).
[1] ISE member.
[2] Tel.: +1 604 221 3087; fax: +1 604 221 3001.

and metal oxides may show low specific surface area, poor electronic and ion conductivity limiting the ES power density. To address these challenges, composite materials have been introduced to ES electrode materials. For example, SC of multi-walled carbon nanotubes (MCNTs) can reach 170 F g^{-1} by introducing polypyrrole [35,36], and if MCNTs are combined with only one percent of RuO$_2$, the SC of such MCNTs can be increased from 30 to 80 F g^{-1} owe to the pseudocapacitive behavior of RuO$_2$ [37]. A polyaniline/carbon nanotube composite electrode [38] with nano-structure, hierarchical porous structure, large surface area, and superior conductivity can have high SC (1030 F g^{-1}), superior rate capability (95% capacity retention at 118 A g^{-1}), and high stability (5.5% capacity loss after 5000 cycles). MnO$_2$/Zn$_2$SnO$_4$/C composite has maximum SC of 643 F g^{-1} at a current density of 1.0 A g^{-1} in 1 M Na$_2$SO$_4$, excellent specific energy of 36.8 Wh kg^{-1}, specific power of 32 kW kg^{-1} at 40 A g^{-1} as well as good long-term cycling stability [39]. In this composite, the crystalline Zn$_2$SnO$_4$ nanowires grown on carbon microfibers which serve as high electrical conductive cores both to support, and provide reliable electrical connections to, the MnO$_2$ shells. Nanostructured Co- and Ni-doped MnO$_2$ deposited using potentiodynamic methods show SC of 621 and 498 F g^{-1}, respectively, at a scan rate of 10 mV s^{-1} [40]. Co(OH)$_2$–Ni(OH)$_2$/Y-zeolite and Co$_x$Ni$_{1x}^-$ layered double hydroxides [42] are two of the most impressive composites with SC of 1710 F g^{-1} [41], and 1809 F g^{-1}, respectively, at a current density of 1 A g^{-1}.

It is obvious that developing composite or hybrid electrode materials has become a new field is also an effective approach to further increase ES electrode material specific capacitance, and in turn improve fES performance. This may be due to the synergistic effect among individual components in the materials through minimizing particle size, enlarging specific surface area, inducing more porosity, and increasing the number of active sites. It is believed that the synergistic effect induced by composites can prevent particle agglomeration, improve electron and proton conduction, and widen the potential window, to improve chemical and mechanical stabilities as well as pseudocapacitances.

In this paper, a nickel and cobalt composite material, Ni$_{0.37}$Co$_{0.63}$(OH)$_2$, was synthesized and characterized using both instrumental and electrochemical methods. An electrochemical reaction mechanism of this material was also proposed based on the electrochemical analyses. The specific capacitance was tested, and the results obtained conclude this material could have a specific capacitance of 1840 F g^{-1} and thus is a potential candidate for ES electrode materials.

2. Experimental

2.1. Material synthesis

For the synthesis of Ni$_{0.37}$Co$_{0.63}$(OH)$_2$ composite materials, analytical grade Co(NO$_3$)$_2 \cdot$6H$_2$O and Ni(NO$_3$)$_2 \cdot$6H$_2$O (Sigma–Aldrich Inc.) and polyethylene glycol 2000 (ALFA AESAR), were used as received. For precursor preparation, the molar ratio of Co(NO$_3$)$_2 \cdot$6H$_2$O and Ni(NO$_3$)$_2 \cdot$6H$_2$O was set at 1:1, and the preparation process was in reference to the one reported by Hu et al. [42], except that the aging time was changed to 24 h. After 24 h of aging, the precipitates formed were filtered and washed with distilled water until the pH of the washed water reached 7.0. The final solid products were then dried at 100 °C in air.

2.2. Characterization

The surface morphologies of the as-prepared samples were observed using a scanning electron microscope (SEM, Hitachi S-3500N) at 20 kV. An auxiliary Energy-dispersive X-ray spectroscope (EDX, Link Isis system, Oxford) was used to confirm composite chemical compositions [43]. The structure and phase analyses were performed using X-ray diffraction (XRD) with Cu Kα1 and Cu Kα2 radiation (Bruker D8 Advance X-ray diffractometer in a Bragg–Brentano configuration). The detected diffraction angle (2θ) was scanned from 10° to 90° with a scan speed of 0.02° s^{-1}. The powder diffraction file database from the International Centre for Diffraction Data was used as a reference to interpret XRD spectra peak distribution.

2.3. Electrochemical evaluation

The electrochemistry of composite material was characterized by cyclic voltammetric (CV) and chronopotentiometric techniques. The measurements were carried out in a conventional three-electrode cell, where a Pt sheet and reversible hydrogen electrode (RHE) were served as the counter electrode and reference electrode, respectively, and Ni$_{0.37}$Co$_{0.63}$(OH)$_2$ coated glassy carbon (geometric surface area of 0.20 cm^2) was as used as the working electrode.

The preparation of working electrodes was as follows: 9.0 mg Ni$_{0.37}$Co$_{0.63}$(OH)$_2$ and 1.0 mg conductive carbon were dispersed ultrasonically in 5.0 ml isopropanol for 30 min to form an ink, then 5.0 μl of this dispersion ink was pipetted gradually onto a pre-polished glassy carbon electrode with a micro syringe. After drying, 5 μl of the diluted Nafion® solution (0.1 wt%, Aldrich) was used to cover this coated glass carbon electrode to form a uniform electrode layer for electrochemical measurements. The electrolyte used in all electrochemical measurements was a N$_2$-saturated 1.0 M NaOH + 0.5 M Na$_2$SO$_4$ solution. To evaluate the effect of pOH on the electrochemical performance of Ni$_{0.37}$Co$_{0.63}$(OH)$_2$, the concentration of NaOH in the electrolyte was adjusted while the concentration of Na$_2$SO$_4$ was kept constant.

Cyclic voltammograms were collected within a potential window of 0–1.5 V (vs. RHE) at a scan rate range of 1–50 mV s^{-1}, using a multi-potentiostat (Solartron 1480) instrument. The reported current densities were normalized to the geometric surface area of the disk electrode. All electrochemical experiments were conducted at room temperature (23 $\pm$ 2 °C) and atmospheric pressure. The specific capacitance was evaluated from the area under the charge and discharge curves from the CV measurements. For charge/discharge tests using chronopotentiometry, a constant current was applied between 0.8 and 1.5 V vs. RHE.

3. Results and discussion

3.1. EDX, SEM and XRD characterization

EDX is used to identify the compositions of the composite materials. Fig. 1 shows the EDX analysis image of composite Ni$_x$Co$_y$(OH)$_2$. According to the collected data from Fig. 1, the atomic ratio of Co to Ni in the composite equals 63:37. This suggests that Ni$_x$Co$_y$(OH)$_2$ may exist in the form of Ni$_{0.37}$Co$_{0.63}$(OH)$_2$ if both nickel and cobalt are divalent.

For morphologies of the synthesized samples, Fig. 2 shows SEM images of Ni$_{0.37}$Co$_{0.63}$(OH)$_2$, Ni(OH)$_2$, and Co(OH)$_2$ for comparison. It can be seen that the average particle size of Ni(OH)$_2$ is about 200 nm, and its basic shape is an aggregate of thin flake. Differing from Ni(OH)$_2$, the shape of Co(OH)$_2$ looks like deformed spheres. For composite Ni$_{0.37}$Co$_{0.63}$(OH)$_2$, it looks similar to Co(OH)$_2$ with larger average sizes than that of Co(OH)$_2$ but still smaller than Ni(OH)$_2$.

Fig. 3 shows the XRD pattern of Ni$_{0.37}$Co$_{0.63}$(OH)$_2$ Ni(OH)$_2$, and Co(OH)$_2$ for structure comparison of the structures. For Ni(OH)$_2$, the XRD pattern shows obvious and sharp peaks at 2θ = 19.1°, 38.8°,
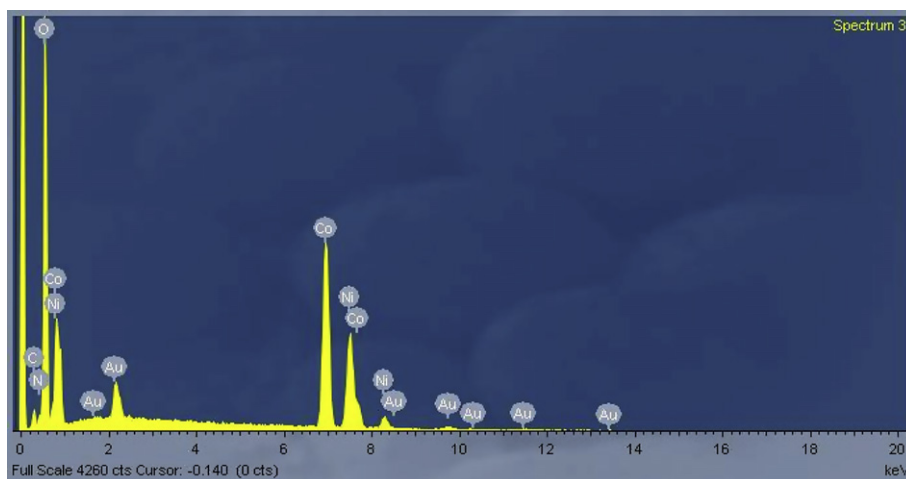
Fig. 1. The EDX analysis image of $Ni_{0.37}Co_{0.63}(OH)_2$.
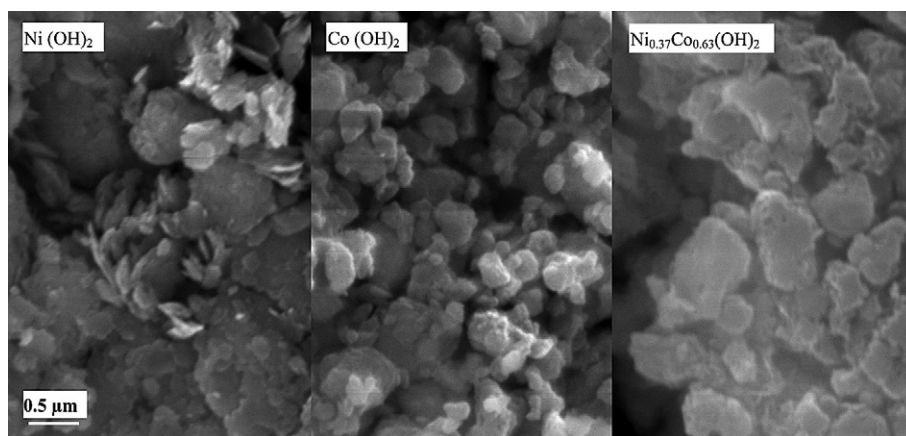
Fig. 2. SEM images of $Ni(OH)_2$, $Co(OH)_2$ and $Ni_{0.37}Co_{0.63}(OH)_2$.

51.8° and 58.9°, respectively, implying a well-crystallized structure as β-$Ni(OH)_2$. For $Co(OH)_2$, no distinct peaks are observed, suggesting that this material has an amorphous nature. Unlike $Co(OH)_2$, $Ni_{0.37}Co_{0.63}(OH)_2$ displays some blurred peaks at $2\theta = 33.3°$ and 59.8°, respectively, suggesting partially formed crystallinity in this material. It is believed that Ni might contribute to these two blurred peaks on the basis of $Ni(OH)_2$ XRD pattern.

3.2. Electrochemical properties of $Ni(OH)_2$, $Co(OH)_2$, and $Ni_{0.37}Co_{0.63}(OH)_2$

Fig. 4 shows the CV curves of $Ni_{0.37}Co_{0.63}(OH)_2$ $Ni(OH)_2$, and $Co(OH)_2$ electrodes, recorded in N_2-saturated 1.0 M NaOH + 0.5 M Na_2SO_4 electrolyte at a potential scan rate of 1.0 mV s^{-1}. It can be seen that the surface anodic reaction peak for $Ni_{0.37}Co_{0.63}(OH)_2$ is

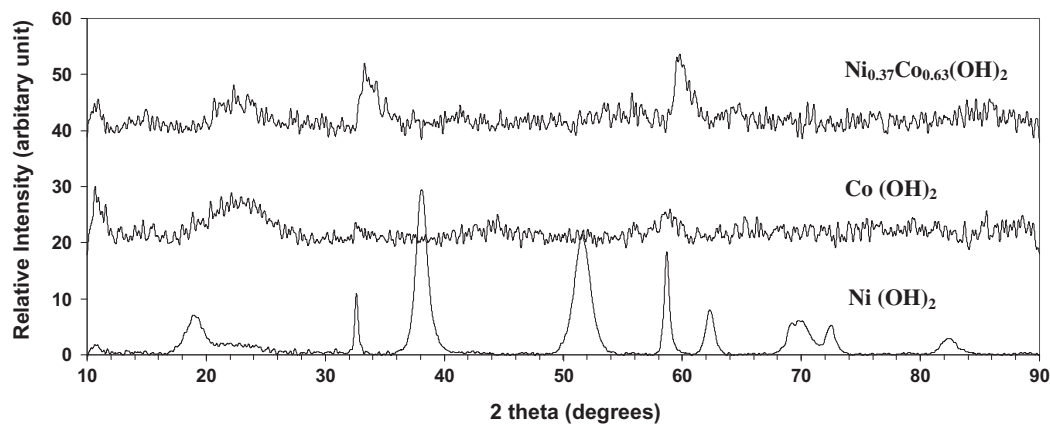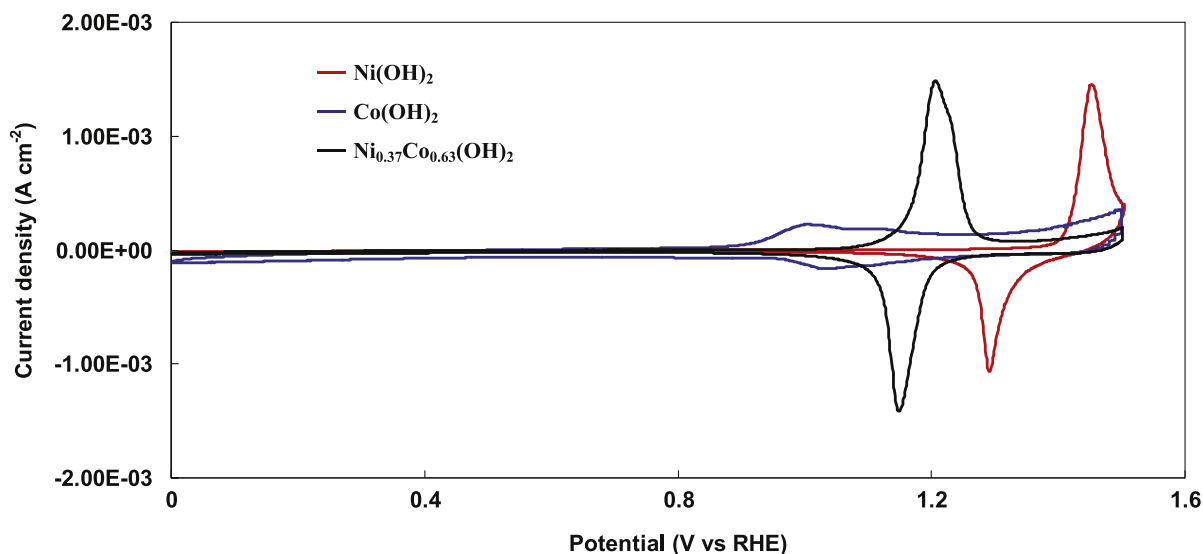**Fig. 3.** XRD patterns of $Ni(OH)_2$, $Co(OH)_2$ and $Ni_{0.37}Co_{0.63}(OH)_2$.

Fig. 4. Cyclic voltammograms of Ni(OH)$_2$, Co(OH)$_2$ and Ni$_{0.37}$Co$_{0.63}$(OH)$_2$ electrodes in N$_2$-saturated 1.0 M NaOH + 0.5 M Na$_2$SO$_4$ electrolyte at a potential scan rate of 1.0 mV s^{-1}. Electrode material loading: 45 g cm^{-2} for all samples.

located near 1.21 V while the cathodic peak is located near 1.15 V. The potential difference ($\sim$50 mV) between the anodic and cathodic peaks is small enough so that it can be considered as a theoretically reversible process. The average redox wave potential is calculated as 1.18 V vs. RHE.

The CVs for the Ni$_{0.37}$Co$_{0.63}$(OH)$_2$ electrode were also recorded at different potential scan rates as shown in Fig. 5. CV curves appear less symmetrical, and the potentials of the anodic and cathodic peaks become more separated, broadening the widths of both anodic and cathodic peaks with increasing potential scan rate. This may imply that parts of the surface of Ni$_{0.37}$Co$_{0.63}$(OH)$_2$ electrode become inaccessible at higher scan rates, probably due to limited ion diffusion and electron transfer within the

electrode. In addition, at higher scan rates, larger potential peak separation between anodic and cathodic peaks may indicate the severity of electrode reaction irreversibility [44].

If peak current density is plotted against potential scan rate, we can clearly see the typical reversibility feature of the Ni$_{0.37}$Co$_{0.63}$(OH)$_2$ redox reaction. Fig. 6 shows the average peak current densities of the Ni$_{0.37}$Co$_{0.63}$(OH)$_2$ electrode as a function of potential scan rate. It can be seen that in the potential scan rate range of <10 mV s^{-1}, the relationship is linear; however, when the scan rate exceeds 10 mV s^{-1}, the peak current density does not follow the linear relationship which implies that Ni$_{0.37}$Co$_{0.63}$(OH)$_2$ may not be electrochemically accessible any more. This liner relationship at scan rates less than 10 mV s^{-1} can be theoretically predicted for
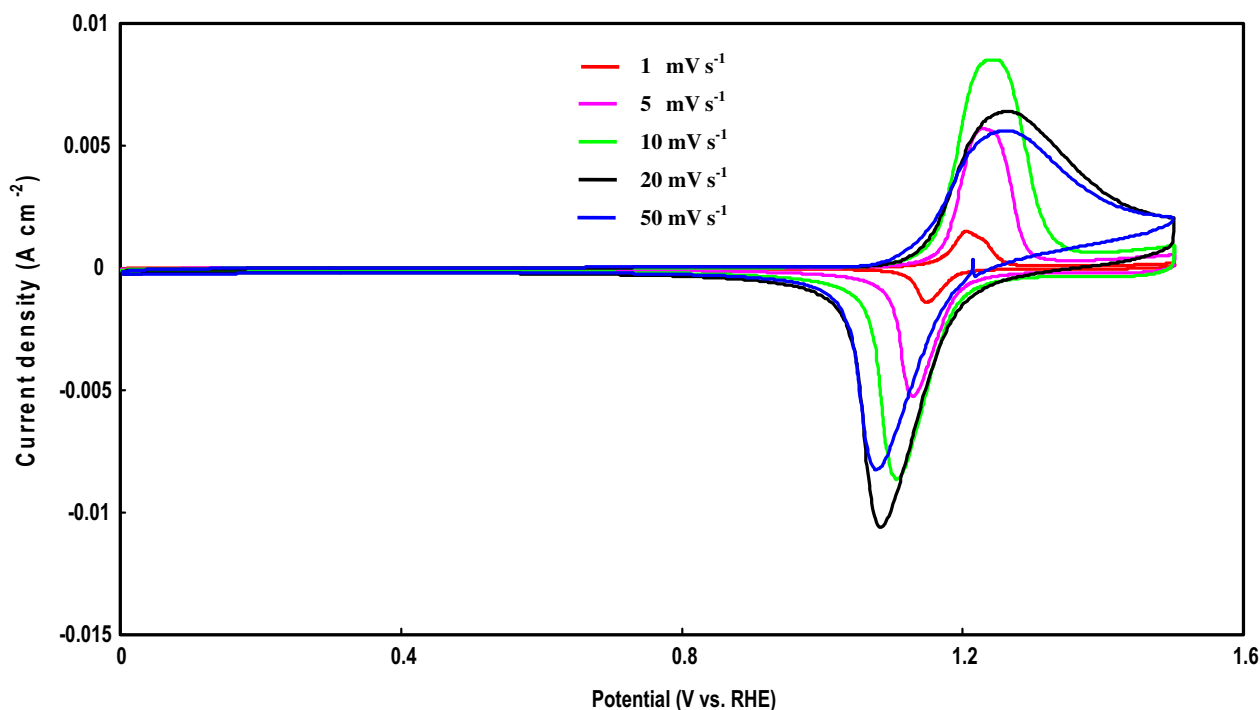

Fig. 5. Cyclic voltammograms of Ni$_{0.37}$Co$_{0.63}$(OH)$_2$ electrode at various potential scan rates in N$_2$-saturated 1.0 M NaOH + 0.5 M Na$_2$SO$_4$. Electrode material loading: 45 g cm^{-2}.
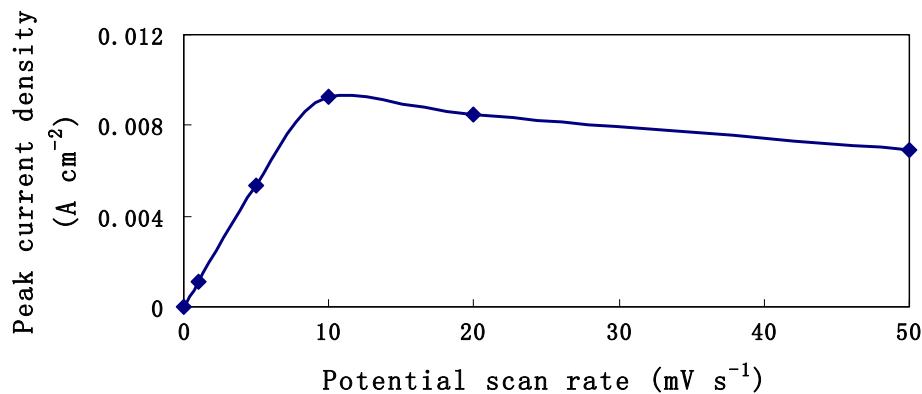
Fig. 6. Peak current densities of $Ni_{0.37}Co_{0.63}(OH)_2$ coated electrode as a function of potential scan rate. Data obtained from Fig. 5.

a surface-confined redox process with all active redox sites completely reactive. This result suggests that in the potential scan rate range of <10 mV s^{-1}, the entire $Ni_{0.37}Co_{0.63}(OH)_2$ electrode layer is accessible by both electrons and OH$^-$ ions; in other words, the entire electrode layer is electrochemically active. The average peak current can be expressed as a function of potential scan rate by Eq. (1) [45]:

$$I_p = \frac{Z^2 F^2}{4RT} \Gamma \nu \tag{1}$$

where Z is the electron transfer number involved in the electrochemical reaction, F is the Faraday constant, R is the gas constant, T is the temperature, ν is the potential scan rate, and Γ is the surface concentration of the active species. Since the Γ is known (4.85×10^{-7} mol cm^{-2}), using Eq. (1), the electron transfer number, Z, involved in the electrochemical reaction of $Ni_{0.37}Co_{0.63}(OH)_2$ can be obtained as 1.9. This result indicates that the electrochemical reaction of $Ni_{0.37}Co_{0.63}(OH)_2$ may be a 2-electron process.

In order to confirm this result, the respective areas under the anodic and cathodic peaks of $Ni_{0.37}Co_{0.63}(OH)_2$ are measured and converted into charge quantities according to the current and potential scan rate. The average between anodic and cathodic charges is 0.019 C. This value is then used to calculate the electron number involved in the redox process. In this calculation, Faraday's law is employed:

$$n = \frac{It}{ZF} \tag{2}$$

where n is the number of moles of $Ni_{0.37}Co_{0.63}(OH)_2$ on the electrode, I is the current, and t is the charge or discharge time. In this case, It is the average charge value (0.019 C), and the number of moles of $Ni_{0.37}Co_{0.63}(OH)_2$ loaded on the electrode is 9.69×10^{-8} mol. Substituting these two numbers into Eq. (2), the electron number of 2.0 can be obtained, which is close to the value obtained from Eq. (1), further confirming that the electrochemical process of $Ni_{0.37}Co_{0.63}(OH)_2$ is likely a 2-electron process.

For Ni(OH)$_2$, from Fig. 4 it can be seen that the surface anodic reaction peak is located near 1.46 V, while the cathodic peak is located near 1.29 V. The large potential difference (~ 170 mV) between the anodic and cathodic peaks indicates the corresponding process is not a reversible process. The average redox wave potential is 1.38 V vs. RHE. For Co(OH)$_2$, a much broader redox wave can be observed with an average peak potential ~ 1.07 V vs. RHE. The different redox potentials of Ni(OH)$_2$ (1.38 V) and Co(OH)$_2$ (1.07 V) from $Ni_{0.37}Co_{0.63}(OH)_2$ (1.18 V) imply that $Ni_{0.37}Co_{0.63}(OH)_2$ is not a simple composite compound of Ni(OH)$_2$ and Co(OH)$_2$; instead, a synergetic compound has been obtained, which has different electrochemical properties from their precursors of Ni(OH)$_2$ and Co(OH)$_2$. For example, the electron transfer numbers for both Ni(OH)$_2$ and Co(OH)$_2$ are close to those calculated using the area under their corresponding anodic and cathodic peaks in a similar way described in Eq. (2) while the electron transfer number of $Ni_{0.37}Co_{0.63}(OH)_2$ is close to two.

For both Ni(OH)$_2$ and Co(OH)$_2$, their electrochemical processes can be expressed as Eqs. (3) and (4), respectively:
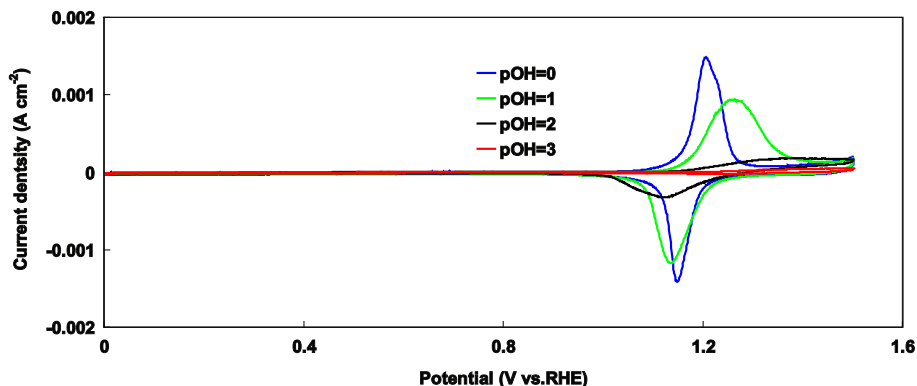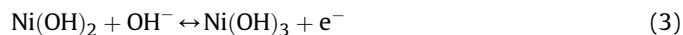
$$Ni(OH)_2 + OH^- \leftrightarrow Ni(OH)_3 + e^- \tag{3}$$

Fig. 7. shows cyclic voltammograms of $Ni_{0.37}Co_{0.63}(OH)_2$ electrode at various pOH in N$_2$-saturated 0.5 M Na$_2$SO$_4$ electrolyte at a potential scan rate of 1.0 mV s^{-1}. Electrode material loading: 45 g cm^{-2}.
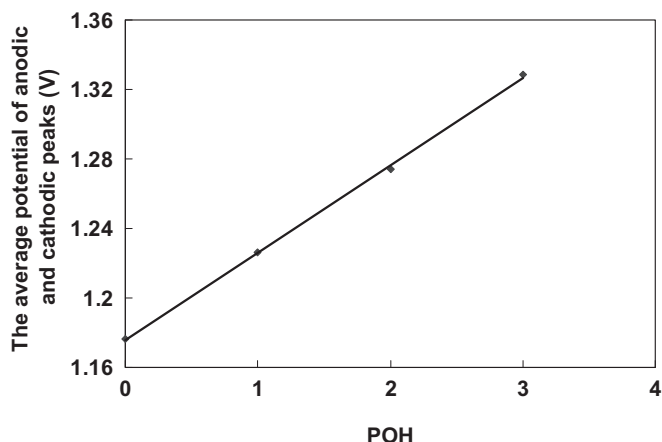
Fig. 8. pOH dependency of the average potential of anodic and cathodic peaks. Data from Fig. 7.
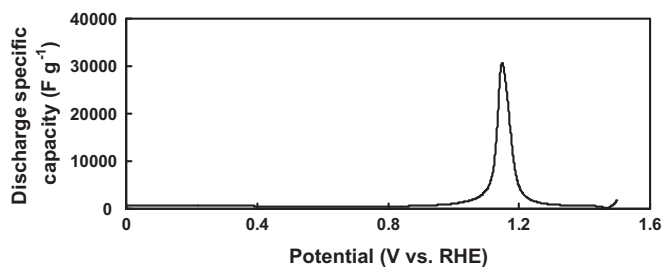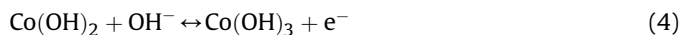

Fig. 9. Discharge specific capacitance vs. potential. Potential scan rate is 1 mV s⁻¹.

$$Co(OH)_2 + OH^- \leftrightarrow Co(OH)_3 + e^- \tag{4}$$

3.3. pOH effect on the electrochemical reaction of Ni₀.₃₇Co₀.₆₃(OH)₂
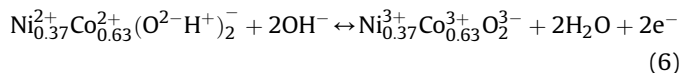
In the electrochemical process of a $Ni_{0.37}Co_{0.63}(OH)_2$ electrode, OH^- ions play an important role in the reaction mechanism. As shown in Fig. 7, the peak shape significantly varies with changing pOH. It can be seen that the higher pOH of the electrolyte, the wider the peaks of both anode and cathode. In order to quantitatively evaluate the pOH effect, the average peak potentials are plotted as a function of pOH as shown in Fig. 8, and exhibit a linear relationship.

Using linear regression, the relationship between the average redox potential (E) and pOH can be expressed as a straight line described in Eq. (5):

$$E = 1.176 + 0.0504pOH \tag{5}$$

Eq. (5) is a form of the Nernst expression for a reversible electrochemical reaction. The slope of 50.4 mV per pOH, which is close to 59.6 mV per pOH for a theoretical one electron-one OH^- process, suggests that in the 2-electron redox process for $Ni_{0.37}Co_{0.63}(OH)_2$, 2 OH^- ions are involved. Based on the electron transfer and OH^- ion numbers obtained above, the following redox reaction for $Ni_{0.37}Co_{0.63}(OH)_2$ in alkaline solution is proposed as Eq. (6):

$$Ni_{0.37}^{2+}Co_{0.63}^{2+}(O^{2-}H^+)_2^- + 2OH^- \leftrightarrow Ni_{0.37}^{3+}Co_{0.63}^{3+}O_2^{3-} + 2H_2O + 2e^- \tag{6}$$

Note that the bi-oxygen group in the compound $Ni_{0.37}Co_{0.63}O_2$ on the right side of Eq. (6) has three negative charges. The structure of $Ni_{0.37}Co_{0.63}O_2$ may contain an oxygen bridge: $[-Ni_{0.37}-O-Co_{0.63}-O-]$ similar to those of Ni^{3+}-based compounds [46].

The electrode potential (E) for Eq. (6) can be written as Eq. (7) according to the Nernst theory:

$$E = E^o + \frac{2.303RT}{2F} \log\left(\frac{a_{Ni_{0.37}Co_{0.63}O_2} a_{H_2O}^2}{a_{Ni_{0.37}Co_{0.63}(OH)_2} a_{OH^-}^2}\right) \tag{7}$$

As $a_{Ni_{0.37}Co_{0.63}(OH)_2}$, $a_{Ni_{0.37}Co_{0.63}O_2}$, and a_{H_2O} are all equal to 1, Eq. (7) can be simplified as Eq. (8):

$$E = E^o - \frac{2.303RT}{F} \log(a_{OH^-}) = E^o + \frac{2.303RT}{F}pOH \tag{8}$$

According to Eq. (5), E^o in Eq. (8) is calculated to be 1.176 V vs. RHE, which is consistent with the experimentally obtained potential of 1.18 V from Fig. 4. The agreement between the expressions derived from the experiment (Eq. (5)) and proposed reaction (Eq. (6)) demonstrates the validity of the proposed redox mechanism (Eq. (6)).
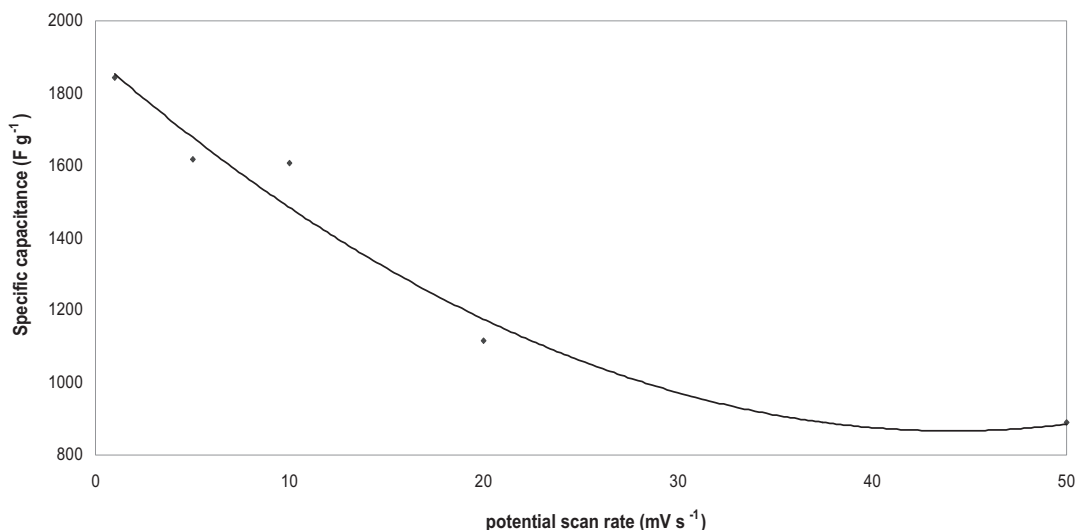

Fig. 10. Specific capacitance as a function of potential scan rate. Electrolyte: N₂-saturated 0.5 M Na₂SO₄. Electrode material loading: 45 g cm⁻².
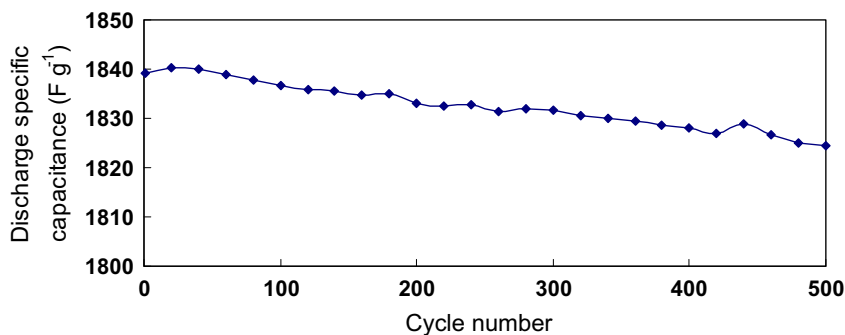
Fig. 11. Cycle stability of $Ni_{0.37}Co_{0.63}(OH)_2$ at 1 mV s^{-1}.

In addition, it can be seen from Fig. 7 that solutions with a pOH higher than 3 may not be suitable as an electrolyte because the low OH^- concentration can cause the surface redox process to be unfavorable, resulting in low specific capacitance.

3.4. Specific capacitance of $Ni_{0.37}Co_{0.63}(OH)_2$

According to cyclic voltammograms (CVs) shown in Fig. 4, the specific capacitance of the $Ni_{0.37}Co_{0.63}(OH)_2$ electrode layer (C_{EL} with a unit of F g^{-1}) can be calculated using Eq. (9):

$$C_{EL} = \frac{Q_{V_1 \leftrightarrow V_2}}{W_{EL}|V_2 - V_1|} \tag{9}$$

where V_1 and V_2 are the low and high end potentials in CV, $|V_1 - V_2|$ is the potential window, $Q_{V_1 \leftrightarrow V_2}$ is half of total charge quantity within the CV curve, and W_{EL} is the total weight of $Ni_{0.37}Co_{0.63}(OH)_2$ and conductive carbon. Two components contribute to C_{EL}: $Ni_{0.37}Co_{0.63}(OH)_2$ through the electrochemical reaction, followed by the conductive carbon inside the electrode layer. Normally, compared to $Ni_{0.37}Co_{0.63}(OH)_2$, the contribution of conductive carbon is negligible. Therefore, in the potential window of 0.0–1.5 V (Fig. 4), the calculated specific capacitance based on the weight of $Ni_{0.37}Co_{0.63}(OH)_2$ is 1840 F g^{-1}. However, the measurement of intrinsic specific capacitance of one material needs the redox reaction potential window. For the intrinsic specific capacitance of $Ni_{0.37}Co_{0.63}(OH)_2$ material ($C_{Ni_{0.37}Co_{0.63}(OH)_2}$), the following Eq. (10) is defined:

$$C_{Ni_{0.37}Co_{0.63}(OH)_2} = \frac{Q_{Ni_{0.37}Co_{0.63}(OH)_2}}{W_{Ni_{0.37}Co_{0.63}(OH)_2}\Delta E} \tag{10}$$

where $Q_{Ni_{0.37}Co_{0.63}(OH)_2}$ is the experimental average charge quantity of anodic and cathodic redox charge quantities calculated from the areas under both anodic and cathodic redox peaks in Fig. 4, $W_{Ni_{0.37}Co_{0.63}(OH)_2}$ is the weight of $Ni_{0.37}Co_{0.63}(OH)_2$ in the electrode layer, and ΔE is the potential difference between the on-set and end-set potentials for the respective anodic and cathodic peaks. The calculated intrinsic specific capacitance of $Ni_{0.37}Co_{0.63}(OH)_2$ is 12,086 F g^{-1}. Moreover, if the discharge SC is plotted against the potential as shown in Fig. 9, the composite material, $Ni_{0.37}Co_{0.63}(OH)_2$, shows an even higher discharge SC within its redox reaction potential window.

Charge/discharge properties are one of the most important factors in determining the power density for supercapacitor electrode materials. A good electrode material provides fast charging/discharging properties. It can be supported by measuring the specific capacitance as a function of potential scan rate. Fig. 10 shows the relationship between $Ni_{0.37}Co_{0.63}(OH)_2$ electrode specific capacitance and potential scan rate. It shows that the specific capacitance decreases with increasing potential scan rate. For example, as the scan rate increases from 1 to 50 mV s^{-1}, the specific capacitance of $Ni_{0.37}Co_{0.63}(OH)_2$ decreases from 1840 to 890 F g^{-1}. This result indicates that at low scan rate the electrode material can be fully utilized while at higher scan rates, portions of the electrode layer active sites are not accessible for redox processes. The decrease in specific capacitance with increasing potential scan rate also implies that if $Ni_{0.37}Co_{0.63}(OH)_2$ is used to
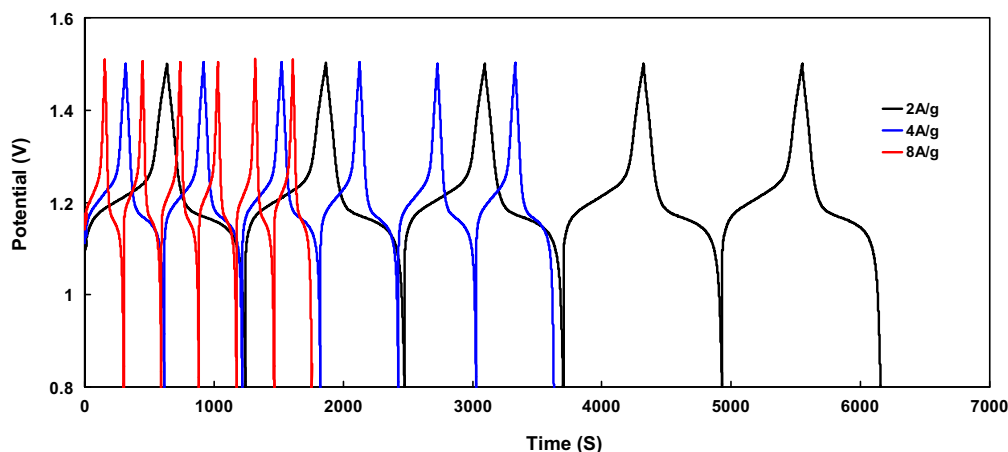

Fig. 12. First six charge–discharge cycles of $Ni_{0.37}Co_{0.63}(OH)_2$ composite electrode in N_2-saturated 1.0 M NaOH + 0.5 M Na_2SO_4 with a potential window of 0.8–1.5 V (vs. RHE) at the current densities of 2, 4 and 8 A g^{-1}. Electrode material loading: 45 g cm^{-2}.

construct a supercapacitor, the charging/discharging process will be limited to low potential scan rates.

Cycle life is another important factor for supercapacitor electrode materials. As shown in Fig. 11, $Ni_{0.37}Co_{0.63}(OH)_2$ displays a high cycle stability at 1 mV s^{-1}. After 500 cycles, $Ni_{0.37}Co_{0.63}(OH)_2$ shows only a specific capacitance loss by 0.8%, suggesting that repetitive charging/discharging would not cause a significant degradation in $Ni_{0.37}Co_{0.63}(OH)_2$ microstructure.

Fig. 12 displays typical charge–discharge curves with mirror-like symmetry for a $Ni_{0.37}Co_{0.63}(OH)_2$ composite electrode at various current densities. The plateaus between 1.16 and 1.22 V imply redox reactions for $Ni_{0.37}Co_{0.63}(OH)_2$, which are also observed in Fig. 4. Fig. 12 also shows lower current densities resulting in longer charging–discharging times due to higher specific capacitances that are consistent with the trend in Fig. 10. From charge–discharge curves, the specific capacitances are calculated as 1770, 1730 and 1700 F g^{-1} at current densities of 2, 4 and 8 A g^{-1}, respectively.

4. Conclusion

In this study, a composite $Ni_{0.37}Co_{0.63}(OH)_2$ material was synthesized via a chemical precipitation method with the purpose to develop electrode materials for supercapacitors. Instrumental methods such as XRD, EDX, and SEM were employed to characterize this material. The results showed that $Ni_{0.37}Co_{0.63}(OH)_2$ possesses an amorphous structure, which provides a higher specific capacitance (1840 F g^{-1}). For electrochemical properties of this electrode material, cyclic voltammetric methods were employed to study its redox process in N$_2$-saturated 1.0 M NaOH + 0.5 M Na$_2$SO$_4$ solution. For comparison, both Ni(OH)$_2$ and Co(OH)$_2$ were also tested. The electrochemical measurements showed that $Ni_{0.37}Co_{0.63}(OH)_2$ could give a two-electron redox process accompanied by two OH$^-$ ions. Based on these results, a redox mechanism was thus proposed.

Cyclic voltammogram curves of $Ni_{0.37}Co_{0.63}(OH)_2$ were recorded and used to measure specific capacitances at different potential scan rates. A typical value of SC was 1840 F g^{-1}. The dependence of potential on specific capacitance showed a reduction in specific capacitance with increasing scan rate. It follows if $Ni_{0.37}Co_{0.63}(OH)_2$ was used to construct a supercapacitor, the charging/discharging process will then be limited to low potential scan rates. To validate this material for supercapacitor applications, charging/discharging tests were also conducted, and the results obtained at various charging/discharging rates were consistent with those tested by changing potential scan rates.

Acknowledgements

References

[1] G. Wang, L. Zhang, J. Zhang, Chem. Soc. Rev. (2011). doi:10.1039/c1cs15060j.
[2] C. Largeot, C. Portet, J. Chmiola, P. Taberna, Y. Gogotsi, P. Simon, J. Am. Chem. Soc. 130 (2008) 2730.
[3] R. Kötz, M. Carlen, Electrochim. Acta 45 (2000) 2483.
[4] A. Burke, J. Power Sources 91 (2000) 37.
[5] B.E. Conway, Electrochemical Supercapacitors, Kluwer Academic/Plenum Press, New York, 1999.
[6] B. Babakhani, D.G. Ivey, Electrochim. Acta 55 (2010) 4014.
[7] B. Babakhani, D.G. Ivey, J. Power Sources 195 (2010) 2110.
[8] J. Lee, K. Liang, K. An, Y. Lee, Synth. Met. 150 (2005) 153.
[9] J.R. Miller, Electrochim. Acta 52 (2006) 1703.
[10] J.P. Zheng, J. Electrochem. Soc. 152 (2005) A1864.
[11] C. Yuan, B. Gao, X. Zhang, J. Power Sources 173 (2007) 606.
[12] Y. Chen, C. Hu, Electrochem. Solid State Lett. 6 (2003) A210.
[13] C.C. Hu, C.C. Wang, J. Electrochem. Soc. 150 (2003) A1079.
[14] H.P. Park, O.O. Park, K.H. Shin, C.S. Jin, J.H. Kim, Electrochem. Solid State Lett. 5 (2002) H7.
[15] R.N. Reddy, R.G. Reddy, J. Power Sources 124 (2003) 330.
[16] P. Simon, Y. Gogotsi, Nat. Mater. 7 (2008) 845.
[17] H. Lee, M.S. Cho, I.H. Kim, J.D. Nam, Y. Lee, Synth. Met. 160 (2010) 1055.
[18] D. Choi, P.N. Kumta, J. Electrochem. Soc. 153 (2006) A2298.
[19] E. Frackowiak, S. Delpeux, K. Jurewicz, K. Szostak, D. Cazorla-Amoros, F. Béguin, Chem. Phys. Lett. 361 (2002) 35.
[20] V. Ruiz, C. Blanco, E.R. Piñero, V. Khomenko, F. Béguin, R. Santamaría, Electrochim. Acta 52 (2007) 4969.
[21] C. Peng, S.W. Zhang, D. Jewell, Prog. Nat. Sci. 18 (2008) 777.
[22] C. Peng, J. Jin, G. Chen, Electrochim. Acta 53 (2007) 525.
[23] A. Malinauskas, J. Malinauskiene, A. Ramanavicius, Nanotechnology 16 (2005) 51.
[24] S. Cho, S.B. Lee, Acc. Chem. Res. 41 (2008) 699.
[25] D. Belanger, T. Brousse, J.W. Long, Electrochem. Soc. Interface 17 (2008) 49.
[26] Y.R. Ahn, M.Y. Song, S.M. Jo, C.R. Park, Nanotechnology 17 (2006) 2865.
[27] V.D. Patake, C.D. Lokhande, O.S. Joo, Appl. Surf. Sci. 255 (2009) 4192.
[28] C.C. Hu, Y.H. Huang, K.H. Chang, J. Power Sources 108 (2002) 117.
[29] J. Yan, T. Wei, J. Cheng, Z. Fan, M. Zhang, Mater. Res. Bull. 45 (2010) 210.
[30] J. Jiang, A. Kucernak, Electrochim. Acta 27 (2002) 2381.
[31] P.A. Nelson, J.R. Owen, J. Electrochem. Soc. 150 (2003) 1313.
[32] U.M. Patil, R.R. Salunkhe, K.V. Gurav, C.D. Lokhande, Appl. Surf. Sci. 255 (2008) 2603.
[33] S.G. Kandalkar, J.L. Gunjakar, C.D. Lokhande, Appl. Surf. Sci. 254 (2008) 5540.
[34] L. Cao, F. Xu, Y.Y. Liang, H.L. Li, Adv. Mater. 16 (2004) 1853.
[35] M. Hughes, M.S.P. Shaffer, A.C. Renouf, C. Singh, G.Z. Chen, D.J. Fray, A.H. Windle, Adv. Mater. 14 (2002) 382.
[36] M. Hughes, G.Z. Chen, M.S.P. Shaffer, D.J. Fray, A.H. Windle, Chem. Mater. 14 (2002) 1610.
[37] G. Arabale, D. Wagh, M. Kulkarni, I.S. Mulla, S.P. Vernekar, K. Vijayamohanan, A.M. Rao, Chem. Phys. Lett. 376 (2003) 207.
[38] H. Zhang, G. Cao, Z. Wang, Y. Yang, Z. Shi, Z. Gu, Electrochem. Commun. 10 (2008) 1056.
[39] L. Bao, J. Zang, X. Li, Nano Lett. 11 (2011) 1215.
[40] K.R. Prasad, N. Miura, Electrochem. Commun. 6 (2004) 1004.
[41] Y.Y. Liang, S.J. Bao, H.L. Li, J. Solid State Electrochem. 11 (2007) 571.
[42] Z.A. Hu, Y.L. Xie, Y.X. Wang, H.Y. Wu, Y.Y. Yang, Z.Y. Zhang, Electrochim. Acta 54 (2009) 2737.
[43] V. Subramanian, H. Zhu, R. Vajtai, P.M. Ajayan, B. Wei, J. Phys. Chem. B 109 (2005) 20207.
[44] J.F. Ni, H.H. Zhou, J.T. Chen, X.X. Zhang, Mater. Lett. 59 (2005) 2361.
[45] A.J. Bard, L.R. Faulkner, Electrochemical Methods, Fundamentals and Applications, Wiley, New York, 1980.
[46] W.S. Cardoso, V.L.N. Dias, W.M. Costa, I.A. Rodrigues, E.P. Marques, A.G. Sousa, J. Boaventura, C.W.B. Bezerra, C. Song, H. Liu, J. Zhang, A.B. Marques, J. Appl. Electrochem. 39 (2009) 55.